Proton transfer and the mobilities of the H^+ and OH^- ions from studies of a dissociating model for water

Song Hi Lee[1,a)] and Jayendran C. Rasaiah[2,b)]
[1]*Department of Chemistry, Kyungsung University, Pusan 608-736, South Korea*
[2]*Department of Chemistry, University of Maine, Orono, Maine 04469, USA*

(Received 1 June 2011; accepted 12 August 2011; published online 26 September 2011)

Hydrogen (H^+) and hydroxide (OH^-) ions in aqueous solution have anomalously large diffusion coefficients, and the mobility of the H^+ ion is nearly twice that of the OH^- ion. We describe molecular dynamics simulations of a dissociating model for liquid water based on scaling the interatomic potential for water developed by Ojamäe-Shavitt-Singer from *ab initio* studies at the MP2 level. We use the scaled model to study proton transfer that occurs in the transport of hydrogen and hydroxide ions in acidic and basic solutions containing 215 water molecules. The model supports the Eigen-Zundel-Eigen mechanism of proton transfer in acidic solutions and the transient hyper-coordination of the hydroxide ion in weakly basic solutions at room temperature. The free energy barriers for proton transport are low indicating significant proton delocalization accompanying proton transfer in acidic and basic solutions. The reorientation dynamics of the hydroxide ion suggests changes in the proportions of hyper-coordinated species with temperature. The mobilities of the hydrogen and hydroxide ions and their temperature dependence between 0 and 50 °C are in excellent agreement with experiment and the reasons for the large difference in the mobilities of the two ions are discussed. The model and methods described provide a novel approach to studies of liquid water, proton transfer, and acid-base reactions in aqueous solutions, channels, and interfaces. © *2011 American Institute of Physics*. [doi:10.1063/1.3632990]

I. INTRODUCTION

Proton transfer is of importance in many chemical reactions and biomolecular processes. The structural diffusion of H^+ and OH^- ions arises mainly from proton transfer (PT) between a solvated ion and a neighboring water molecule. It has been studied extensively by *ab initio* molecular dynamics (AIMD) (Refs. 1–6) and applications of extended valence bond theory (EVB).[7–12] A reactive molecular dynamics algorithm has also been proposed to study proton transport.[13] The solvation structures of H^+ and OH^- ions have been probed by neutron[14–20] and x-ray diffraction,[21] x-ray adsorption,[22] and spectroscopy experiments[23–32] that explore the structures and excitations (vibrational, rotational, and electronic) of equilibrium and transition states in proton transfer reactions. A theoretical framework that relates microscopic states to the mechanism and kinetics of PT reactions, and predicts a set of lifetimes and rates of formation and decay of intermediate states that can be verified by time-resolved spectroscopy has been proposed.[33] Accounts and commentaries describing mechanisms and simulations of PT have appeared,[34–43] and a comprehensive review of structural diffusion in the context of PT, with special reference to the hydroxide ion covering the field up to mid-2009 was published recently.[44]

It is well known that the diffusion coefficients of the hydrogen and hydroxide ions are anomalously large and the mobility of the H^+ ion is nearly twice that of the hydroxide ion. Marx *et al.*[2] employed AIMD to study the solvation and diffusion of hydrogen ions, with forces computed "on the fly" using density functional theory (DFT) and the BLYP exchange functional. Similar methods were used by Tuckerman *et al.*[3,39] to study hydroxide ions in aqueous solution. The nature of the hydrogen ion in aqueous solution, consisting of the Eigen (E) and Zundel (Z) complexes and other intermediates, and the mechanism of transport that involves proton transfer from Eigen to Zundel to Eigen structures (the Eigen-Zundel-Eigen (EZE) sequence) driven by solvent fluctuations followed by "presolvation" is well understood,[1,2,27,34–36] but there have been conflicting opinions about the structure of the hydrated hydroxide ion and the mechanism of transport.[3–5,45] The BLYP functional in DFT calculations favors four-coordinated hydration of OH^- at room temperature,[3] while a different functional (PW91) supports a three-coordinated complex[5] formed by hydrogen bonding with water molecules along the three lone pairs of the oxygen atom in OH to produce a canonical Lewis structure. Four-coordinated hydration, postulated by the BLYP functional, has its origin in a delocalized ring of charge that replaces the directed lone pairs.[3] The oxygen atom accepts an additional water molecule via H-bonding to form a roughly square planar arrangement of water molecules on the side opposite to the hydrogen atom of the OH^- ion to form $OH^-(H_20)_4$. The hydrogen atom of this ion is also transiently H-bonded to a fifth water molecule and on average, a hyper-coordinated complex with four H-bonds accepted and one donated is postulated with an overall coordination number of 4.5.[3]

The difference in solvation structures postulated by the BLYP and PW91 functionals, translates into different mechanisms for structural diffusion; and the PW91 functional

a)Electronic mail: shlee@ks.ac.kr.
b)Electronic mail: rasaiah@maine.edu.

predicts a larger OH^- ion mobility than the experimental mobility at room temperature.[39] A different solvation structure (also 4-coordinated) is predicted by the HCTH exchange functional leading to another mechanism for the structural diffusion of the OH^- ion but with a diffusion coefficient that is smaller than that of liquid water which contradicts the experimental facts.[39] Tuckerman *et al.*[39] also showed that the order of the diffusion coefficients for H^+ and OH^- is reversed when the PW91 functional is used in DFT/AIMD simulations with the diffusion coefficient of the hydroxide ion greater than that of the hydrogen ion. Of the three, the BLYP functional gives the correct experimental order.

There is experimental evidence in support of both 3- and 4- (or hyper-)coordinated species with suggestions that their proportions vary with temperature such that the 4-coordinated structure is dominant at room temperature.[19,20,28] Chandra *et al.* analyzed the available experimental data using their theoretical framework and found that the experimental lifetimes at room temperature were consistent with the predictions of the BLYP functional supporting the hyper-coordinated structure of the OH^- ion and a mechanism of structural diffusion ("dynamic hyper-coordination") based on this structure.[33,44]

Newer and improved density functionals have been proposed for water,[46] but the effect of temperature on accuracy of the AIMD simulations of PT using a specific exchange functional is difficult to predict.[47] Ufimstev *et al.* proposed a charged ring model to represent the delocalized ring of charge in the OH^- ion.[48] The model predicts a distribution of 4- and 3-coordinated complexes and provides the base states of a multistate EVB force field in their studies of proton transfer in basic solution. Like other EVB methods, the computations are less demanding than *ab initio* calculations.

Here we discuss a different model that uses a single force field to study the dynamics of proton transfer and the solvation structure of both hydrogen and hydroxide ions in aqueous solution. Our calculations are based on scaling the Ojamäe-Shavitt-Singer (OSS) (Ref. 49) potential for water, and are easily adapted to conventional molecular dynamics (MD) simulations even on a large scale. The OSS2 potential is a central force model[50–52] for water that incorporates dissociation into hydrogen and hydroxide ions, and was derived from *ab initio* studies of protonated water dimers and clusters at the MP2 level. However, the original OSS2 model is unsuitable for the bulk liquid since it represents a supercooled or glassy state with a negligible diffusion coefficient.[53] Normal diffusion in the bulk phase emerges at lower densities ($\sim$0.5 g cm^{-3}) and higher temperatures ($\sim$500 K) (Ref. 53) suggesting that the OSS2 potential can be scaled for use under ambient conditions. We accomplish this by exploiting the coupling between the inverse temperature and the potential in the partition function and call it the scaled OSS2 (or sOSS2) model. The model supports the EZE mechanism of proton transfer in weakly acidic aqueous solutions and a mix of hyper-coordination (4 accepted and 1 weakly donated) and four coordination (4 accepted and none donated or 3 accepted and 1 donated) of the hydroxide ion in weakly basic solutions at room temperature with an average coordination number of $\sim$4.6. The reorientation dynamics of the OH^- suggests that the proportions of these structures change with temperature between 0 and 50 °C. The free energy barriers for proton transport are small for both H^+ and OH^- ions and the proton is more significantly delocalized in the weakly acidic solution as shown previously in path integral simulations.[3,44] A Zundel-like transition state occurs for PT towards the OH^- with a lifetime comparable to what has been reported experimentally. The calculated diffusion coefficients as a function of temperature between 0 and 50 °C are in good agreement with experiment.

This paper is organized as follows. In Sec. II we describe scaling of the OSS2 model for water. Section III discusses the use of the scaled model (sOSS2) to study proton transfer in acidic and basic solutions and details of the solvation structures during proton transfer. Section IV is about the reorientation dynamics of the solvated OH^- ion, and Sec. V discusses the mobility of the H^+ and OH^- ions at 0.26 M as a function of temperature from 0 to 50 °C and makes comparisons with experiment. The conclusions are in Sec. VI.

II. SCALING THE OSS2 MODEL

To describe the scaling, suppose that T' is the temperature at which the equilibrium properties of the OSS2 model match those of real water at room temperature (T = 298.15 K) and density, where we observe from our simulations that $T' > T$. Multiplying the OSS2 potential V_{OSS2} by the factor $\beta' = 1/kT'$ in the partition function (k is the Boltzmann's constant) is equivalent to scaling the OSS2 potential by a factor $\lambda = T/T'$ at the temperature T as in thermodynamic perturbation theory.[54,55] The scaled OSS2 potential is thus defined by $V_{sOSS2} = \lambda V_{OSS2}$; where the parameter λ determines V_{sOSS2} from the OSS2 potential.[49] Small changes in λ are then made to get the optimal results as described below. The method is deceptively simple but has only a partial quantum mechanical basis since it is obtained by scaling the OSS2 potential derived from *ab initio* simulations at the MP2 level.[49]

The OSS2 potential model has been described by Ojamäe *et al.*[49] and details of our simulation methods for this potential are summarized in Ref. 53. The same methods were used here for the sOSS2 potential. Our MD simulations were performed in the NVT ensemble with the number of water molecules N $\sim$ 215 and the temperature controlled by a Nose-Hoover thermostat.[56] The new feature is the scaling factor λ that defines the scaled potential $V_{sOSS2.}$ This requires scaling the charge q_i of particle i by the square root of λ ($q_i' = \lambda^{1/2} q_i$) in calculations of the electrostatic energy, while the induced dipole moment at each oxygen site is obtained self-consistently in the same way as it was before scaling.[49,53] The other three non-electrostatic potential energies (V_{OH}, V_{OO}, and V_{HOH}) in the OSS2 potential were also scaled by λ. Ewald summations are used in our simulations with the parameter for $\kappa = 5.0/L$ and the real-space cut distance r_{cut} and K_{max} chosen as 0.5L and 7, respectively, where L is the length of the box ($\sim$18.64 Å for 216 water). The double summations in reciprocal space, which cannot be reduced to a single summation due to the cutoff functions, were ignored. This is reasonable as the distances in reciprocal space are larger than the length L of the box. The velocity Verlet algorithm[57] was employed

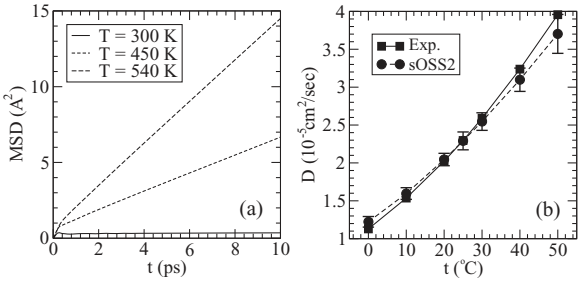

FIG. 1. (a) Mean square displacements (MSD) of the OSS2 water at several different temperatures. Solid line: at 300 K, dotted line: at 450 K, and long-dashed line: 540 K all at a density of 0.9970 g/cm^3. (b) Comparison of self-diffusion coefficients of the sOSS2 water at several different temperatures. ■: experimental values (Refs. 60 and 61), and ●: calculated values for 216 water molecules using the sOSS2 potential. The error bar represents a standard deviation.

TABLE II. Relaxation times (τ in ps) and activation energies E_a (kJ/mol) for reorientation of the OH bond in the sOSS2 model for water and OH^- ion in sOSS2 water between 0 and 50 °C.

Temp. (°C)	Water (OH bond) (ps)	OH^- ion (ps)
0	4.8 ± 0.5	11.3 ± 0.6
10	3.9 ± 0.5	6.9 ± 0.6
20	3.0 ± 0.5	4.2 ± 0.4
25	2.6 ± 0.5	3.2 ± 0.4
30	2.4 ± 0.4	2.9 ± 0.3
40	1.9 ± 0.5	1.9 ± 0.4
50	1.7 ± 0.4	1.7 ± 0.4
E_a (kJ/mol)	16 ± 2	17 ± 2/34 ± 2[a]

[a]The two activation energies for the OH^- ion are determined from the 3 lower (30–50 °C) and 3 higher (0–20 °C) relaxation times, respectively, see Fig. 2.

for time integration with a time step of 1 fs. The equilibrium properties are averaged over 60–100 blocks of 100 000 time steps and the configuration of all the atoms is stored every 10 time steps for further analyses. The simulations were first validated by checking our results against Ojamäe's work for pure water using the OSS2 model.[49] The calculated oxygen-hydrogen (O-H) radial distribution function and the hydration number n(r) for hydrogen in the 216 molecule pure water system were nearly identical,[58] even though Ojamäe *et al.*[49] used a different method for the Ewald sums in the calculation of the induced dipole moment.

The self-diffusion coefficient is readily determined in a MD simulation from the mean square displacement (MSD), and we use it as a probe to identify the temperature T' at which OSS2 model water has nearly the same properties as liquid water under ambient conditions. The diffusion coefficient D for the OSS2 model at room temperature and fluid density $\rho = 0.9970$ g/cm^3 is near zero (see Fig. 1(a)), but at 540 K the diffusion coefficient is nearly identical to the experimental value for water (2.26×10^{-5}–2.29×10^{-5} cm^2/s (Refs. 59–61)) at 298.15 K. From our scaling hypothesis $\lambda = T/T' = 298.15/540 = 0.552$, and we expect the sOSS2 model at 298.15 K to have nearly the same diffusion coefficient ($2.30 \pm 0.09 \times 10^{-5}$ cm^2/s) as the OSS2 model at 540 K. The diffusion coefficient at 298.15 K from the MSD ($2.00 \pm 0.09 \times 10^{-5}$ cm^2/s) is within 12% of the experimental result. Further fine-tuning by choosing $\lambda = 0.530$ leads to agreement ($D = 2.27 \pm 0.07 \times 10^{-5}$ cm^2/s) to within 1%.

In principle λ has to be re-determined at each temperature T from a new T′, but the change in λ with temperature is small because it is the ratio of two temperatures ($\lambda = T/T'$) that is less sensitive to changes in temperature than the individual temperatures. Figure 1(b) and Table I show that the experimental diffusion coefficients[60,61] of pure water can be predicted to high accuracy between 0 to 50 °C (273 to 323 K) using a single $\lambda = 0.530$ determined at 298.15 K. The activation energy for translational diffusion calculated from the Arrhenius equation $D = D_0 \exp(-E_{trans}/RT)$, is 16 kJ/mol for the sOSS2 model in close agreement with 18 kJ/mol from experimental data.[60,61]

Besides translation, the reorientation of water molecules[62] plays an important role in the dynamics of breaking and forming hydrogen bonds in liquid water.[63–66] We calculated the relaxation times ((τ) for reorientation of the sOSS2 water between 0 to 50 °C (273 to 323 K) from the orientation correlation functions $\langle P_2[\mathbf{u}(t)\cdot\mathbf{u}(0)]\rangle$, where P_2 is the second order Legendre polynomial and $\mathbf{u}(t)$ is the unit vector along the OH bond of a water molecule (Table II). The agreement with NMR reorientation times[62] shown in Fig. 2 is excellent. The activation energies for reorientation were determined from plots of $\log(\tau)$ *vs* 1/T. They are 16 kJ/mol, for rotation about the OH bond in water (sOSS2 model) in good agreement with 14 kJ/mol obtained from the NMR data.

Remarkably the same scaling hypothesis holds for the equilibrium structure as shown in Figs. 3(a), 3(b), and 3(c), where the atom-atom O–O, O–H, and H–H distribution func-

TABLE I. Diffusion coefficients (10^{-5} cm^2/s) of H_2O, H^+, and OH^- ion between 0 °C and 50 °C. Simulations results for sOSS2 model for 0.26 M HCl or NaOH compared with experiment.

Temp. (°C) (Density (g/cc))	H_2O sim (expt.)	H^+ ion sim-0.26 M (expt.)[a]	OH^- ion sim-0.26 M (expt.)[a]
0 (0.9999)	1.22 ± 0.08 (1.129)	4.95 ± 1.34 (6.00)	2.77 ± 0.70 (3.15)
10 (0.9997)	1.60 ± 0.08 (1.536)	6.03 ± 1.59 (7.34)	3.44 ± 0.91 (3.95)
20 (0.9982)	2.05 ± 0.08 (2.023)	7.10 ± 1.57 (8.66)	4.19 ± 1.14 (4.84)
25 (0.9970)	2.27 ± 0.12 (2.290)	7.62 ± 1.59 (9.31)	4.56 ± 1.29 (5.30)
30 (0.9957)	2.55 ± 0.12 (2.590)	8.09 ± 1.66 (9.94)	4.87 ± 1.31 (5.76)
40 (0.9922)	3.10 ± 0.15 (3.238)	9.05 ± 1.68 (11.2)	5.54 ± 1.47 (6.69)
50 (0.9881)	3.70 ± 0.26 (3.956)	10.0 ± 1.78 (12.3)	6.24 ± 1.46 (7.61)
E_a (kJ/mol)	16 (18)	10.3 (10.6)	12.0 (13.0)

[a]Numbers in parenthesis are the experimental results for H^+ and OH^- ions at infinite dilution (Ref. 77).

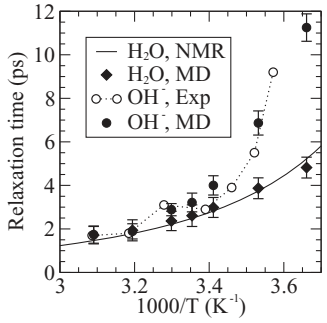

FIG. 2. The orientation relaxation times of water and OH^- ion calculated from $\langle P_2[\mathbf{u}(t)\cdot\mathbf{u}(0)]\rangle$ as function of 1000/T. The solid line is the experimental NMR result for water (Ref. 62) fitted to $\tau_{NMR} = 0.34\ [(T\text{-}223)/223]^{-1.83}$ and the symbols (◆) are MD calculations for sOSS2 water with the unit vector $\mathbf{u}(t)$ along the OH bond. The relaxation times for the OH^- are from MD calculations for the ion in sOSS2 water (●), and from CTTS experiments (Ref. 28) (○) with the unit vector $\mathbf{u}(t)$ along the OH bond.

tions for the sOSS2 potential ($V_{sOSS2} = 0.530\ V_{OSS2}$) are compared with the experimental results for liquid water from neutron and x-ray diffraction data,[67] and distribution functions for the rigid SPC/E model for water[68] at 298.15 K. The peak heights are lowered in moving from the OSS2 to the sOSS2 model potential at room temperature but the positions are nearly the same (not shown). The distribution functions of the sOSS2 model are in good agreement with experiment and are comparable or superior to the SPC/E model, except that the peaks corresponding to dissociation are absent in the SPC/E model, and the rest are shifted to slightly longer distances by ~0.05–0.06 Å. These results taken together suggest that the sOSS2 model represents the equilibrium structure and transport properties of water quite accurately at and near ambient temperatures.

We used the same sOSS2 model, with the predetermined scaling of $\lambda = 0.530$ for liquid water, to study the mobility of H^+ and OH^- ions in 215 water molecules in the presence of either a stationary chloride (Cl^-) or sodium (Na^+) counterion to maintain electro-neutrality. For the system containing a single NaOH, we have 216 O^{2-}, 431 H^+, and a single Na^+ ion. The H^+ ion is not polarizable in the OSS2 model,[49] and we consider the Na^+ ion as an additional (432th) cation (like H^+) that contributes electrostatic and Lennard-Jones (LJ) 6-12 interactions to the total potential with $\varepsilon = 0.6034$ kJ/mol, $\sigma_{Na\text{-}O} = 2.773$ Å,[69] and $\sigma_{Na\text{-}H} = 1.175$ Å assuming $\sigma_{H\text{-}H} = 0$. For the system containing a single HCl, we have 215 O^{2-}, 431 H^+, and a single Cl^- ion. Although O^{2-} is polarizable in the OSS2 model, we treat the Cl^- ion as a nonpolarizable anion that contributes electrostatic and Lennard-Jones interactions to the potential energy of the system with $\epsilon = 0.5292$ kJ/mol, $\sigma_{Cl\text{-}O} = 3.823$ Å,[69] and $\sigma_{Cl\text{-}H} = 2.225$ Å assuming $\sigma_{H\text{-}H} = 0$.

III. PROTON TRANSFER USING THE sOSS2 WATER MODEL

We find that the hydrogen ion exists as a range of structures in liquid water and PT occurs from a central proton in the Eigen complex $H_3O^+(H_2O)_3$ through a Zundel intermediate preceded and followed by solvent reorganization as noted previously in AIMD simulations by Marx *et al.*[2] and theoretical discussions by Agmon[34,35] and others.[36,40–43] The Eigen cation $H_3O^+(H_2O)_3$ (Fig. 4(a)(i)), present before PT occurs, has a second solvation shell around H_3O^+ hydrogen-bonded to the primary shell. Thermal fluctuations break the H-bond of a water molecule in this shell, and prepare the undercoordinated water molecule in the first shell with the oxygen atom designated as O^ from which it was detached, to receive a proton from H_3O^+ characterized as "presolvation."[2,44] This feature is also reproduced in our simulations using the sOSS2 model. Characterizing the oxygen in H_3O^+ as O*, the O* and O^ atoms are linked by a hydrogen bond to form the Zundel complex $[H_2O^*\text{-}H^*\text{-}O^\wedge H_2]^+$ in which the O*-O^ distance has shrunk from 2.67 Å to 2.36 Å. This "most active" H* shuttles between two O's (Fig. 4(a)(ii)) in an essentially barrierless transition as discussed by Agmon[34,35] and Marx *et al.*[2] If the O^ returns to its former state by forming a hydrogen bond with an extraneous water molecule the most active H* atom goes back to O* and PT does not occur (not shown). Alternatively, if the O* atom of the original Eigen complex, now present in the Zundel form, becomes four coordinated by forming a H-bond with a fourth water, the active H* within the Zundel complex moves to O^ and PT occurs to form a new H_3O^+ ion that is stabilized in the next step by the formation of an Eigen complex or undergoes one or more successive PTs. A single PT is completed and stabilized with the configuration shown in Fig. 4(a)(iii).

Following Marx *et al.*[2] we select the displacement coordinate $\delta = R_{O^*H^*}\text{-}R_{O^\wedge H^*}$ to identity the solvated complexes and determine the free energy profile for PT. Here $R_{O^*H^*}$ and $R_{O^\wedge H^*}$ are the respective distances of the shared proton H*

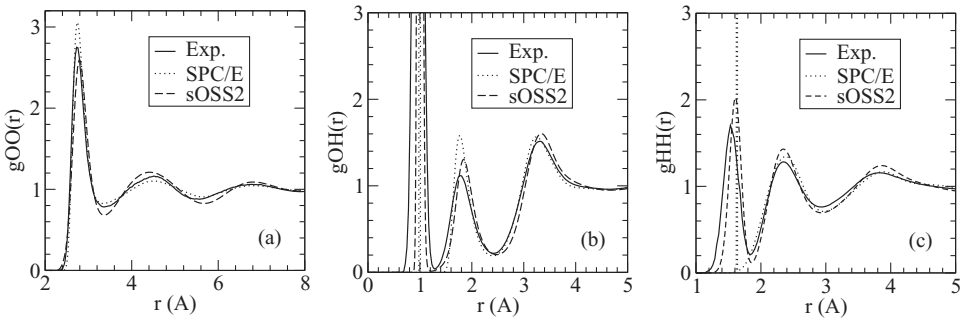

FIG. 3. (a) O–O radial distribution functions at 298 K. Solid line: the experimental result (Ref. 67), dotted line: the SPC/E model (Ref. 68), and dashed line: the sOSS2 model. (b) O–H radial distribution functions at 298 K. (c) H–H radial distribution functions at 298 K.

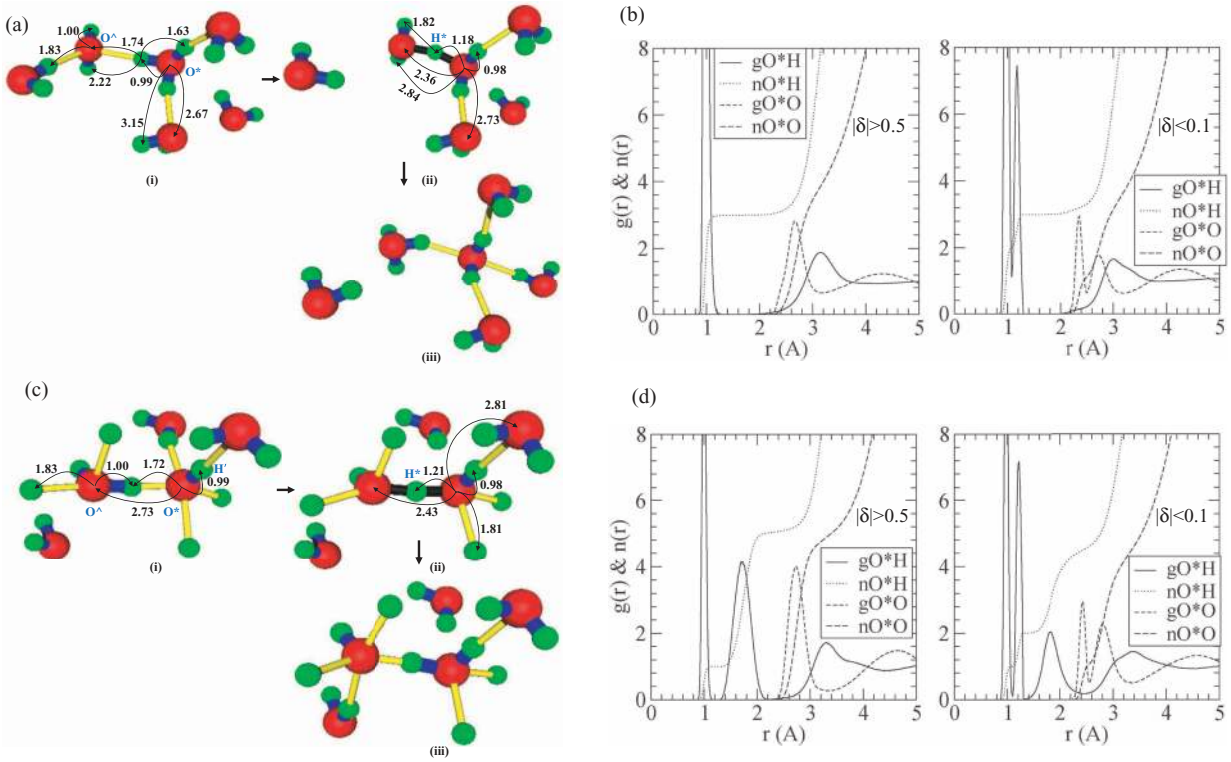

FIG. 4. (a) Representative configurations showing the mechanism of **single** proton transfer leading to the transport of a hydrogen ion in a simulation of one H_3O^+ ion in 215 water molecules using the sOSS2 potential. (i) H_3O^+ ion stabilized as an Eigen complex $H_3O^+(H_2O)_3$ showing three coordination of H_3O^+ and a water molecule in the second solvation shell. (ii) Loss of water in the second solvation shell in (i) and the formation of the Zundel intermediate $H_5O_2^+$. (iii) Completion of proton transfer via the Zundel intermediate to form a new H_3O^+ ion. (b) The radial distribution functions g_{O^*H} and g_{O^*O} and corresponding coordination numbers n_{O^*H} and n_{O^*O} with respect to the oxygen atom O* of the hydrogen ion $H_3O^{*\,+}$ in 215 water molecules for configuration in which the displacement coordinate $|\delta| > 0.5$ Å (left panel) and $|\delta| < 0.1$ Å (right panel). (c). Representative configurations of OH^- ion showing the mechanism of **single** proton transfer leading to the transport of the hydroxide ion in a simulation of one OH^- ion in 215 water molecules using the OSS2 potential. (i) $O^*H'^-(H_2O)_{4.6}$ complex showing four coordination of O*. (ii) $OH^-(H_2O)_3$ intermediate with H' between O* and O^ showing three coordination of O*. (iii) Completion of proton transfer via $OH^-(H_2O)_{4.6}$ intermediate (see the text). (d) The radial distribution functions g_{O^*H} and g_{O^*O} and corresponding coordination numbers n_{O^*H} and n_{O^*O} with respect to the oxygen atom O* of the hydroxide ion O^*H^- in 215 water molecules for configuration in which the displacement coordinate $|\delta| > 0.5$ Å (left panel) and $|\delta| < 0.1$ Å (right panel).

from O* and O^. The sequence of events leading to proton transfer can be understood by examining the conditional distribution functions for two sets of configurations for which $|\delta|$ is small ($|\delta| < 0.1$ Å) or large ($|\delta| > 0.5$ Å). A small $|\delta|$ (right panel of Fig. 4(b) and configuration (ii) of Fig. 4(a)) indicates a potential pathway for proton transfer via a Zundel complex and a large $|\delta|$ (left panel of Fig. 4(b) and configurations (i) and (iii) of Fig. 4(a)) represents states before and after PT.

The running coordination number $n_{O^*H} = 3$ after the first O*-H intra-molecular peak in g_{O^*H} at 0.99 Å in the left panel of Fig. 4(b) ($|\delta| > 0.5$ Å), confirms the presence of three H-atoms bonded to O* in the Eigen complex H_3O^{*+}. The peak in g_{O^*O} at 2.67 Å for large $|\delta| > 0.5$ Å reflects the presence of an oxygen atom in the first coordination shell of the Eigen complex (see the left panel of Fig. 4(b)). When $|\delta|$ is small (right panel of Fig. 4(b)) this peak is split into two, a sharp one at 2.36 Å equal to the O*-O^ distance in the Zundel complex and running coordination number $n_{O^*O} = 1$ and a second peak identifying the oxygen atom of a water molecule in the first solvation shell of O* which has receded to 2.73 Å. The peak in the conditional pair correlation function g_{O^*H} at 0.99 Å for $\delta > 0.5$ Å is also split into two peaks at 0.98 Å and 1.18 Å, respectively, when $\delta < 0.1$ Å with running coordination numbers $n_{O^*\text{-}H}$ of 2 and 3, respectively, consistent with the presence of two chemical bonds and one hydrogen bond associated with the O* atom of the Zundel intermediate. (see configuration (ii) of Fig. 4(a)).

The free energy profile F((δ) shown in Fig. 5(a), for proton transfer within the Zundel state in acidic solution of 0.26 M (Figs. 4(a) and 6(a)), was constructed from the normalized probability distributions P(δ) of the displacement coordinate δ and the relation F((δ) = −kT ln P(δ). The barrier height is 0.14 kcal/mol compared to 0.13 kcal/mol reported in Ref. 44 and is small relative to the average thermal energy of 0.59 kcal/mol at 300 K. The low barrier and the absence of a well at or near the top suggests that the proton is significantly delocalized in the Zundel complex, as suggested earlier by Marx *et al.*,[2] and the energy difference between the Eigen and Zundel forms is small. The lower panel of Fig. 5(b) depicts the proton jump distances every ten time steps over an interval of 100 000 time steps or 100 ps.

In our study using the sOSS2 model, the hydroxide ion at 0.26 M exists mainly as hyper-coordinated structures at 298 K before PT occurs. The solvation of the OH^- ion by water molecules involves four H-bonds accepted by the oxygen atom in a roughly square planar arrangement and

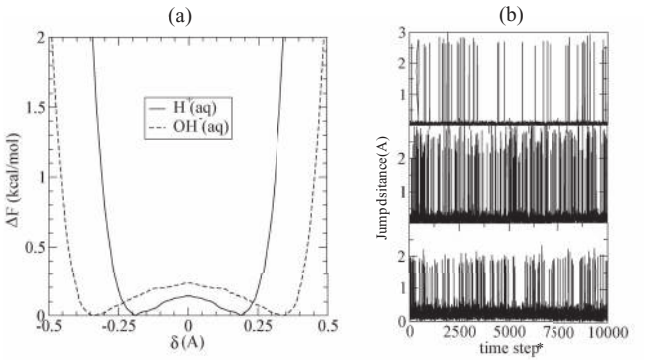

FIG. 5. (a) Free energy profile at 298 K along the proton transfer coordinate δ of the H^+ and OH^- systems. (b) Jump distances of H* of H^+ ion (lower panel), H* of OH^- ion (middle panel), and O* of OH^- ion (lower panel) versus the time step* = time steps/10 where one time step = 1 fs.

one donated by the H atom of the OH^- ion adding up to an overall average coordination number of ~4.6 as noted previously by Tuckerman *et al.*[3] from AIMD simulations of an ion and 31 water molecules (~1.7 M). (see Figs. 4(c) and 6(b)). This structure is supported by neutron and x-Ray diffraction,[19–21] x-ray adsorption,[22] ultrafast and 2D infrared spectroscopy,[29,31] and core-level photoelectron emission studies.[32] In contrast to the AIMD simulations of Tuckerman *et al.*,[3] we find that the hyper-coordinated species exists before the initial PT step. The weaker hydrogen bond donated to the oxygen atom of a neighboring water remains during PT and becomes stronger and part of the first solvation shell of a neighboring water molecule after PT has taken place.

The hydroxide ion moves in a direction opposite to that of proton transfer towards the oxygen of OH^- and occurs in the sequence depicted in Figs. 4(c)(i) to 4(c)(iii). PT of the hydroxide ion starts from the hyper-coordinated $OH^-(H_2O)_{4.6}$ and proceeds through three-coordinated intermediates by losing a water molecule from the roughly square planar arrangement followed by the formation of a Zundel-like transition state $[HO^*\text{-}H\text{-}O^\wedge H]^-$ involving one of the three remaining water molecules hydrogen-bond to O*, the oxygen of OH^-, to which PT may eventually occur. This transition state has been observed recently in spectroscopic studies by Roberts *et al.*[29,31]

The sequence of events in PT to an OH^- is readily followed by selecting two sets of configurations for which $|\delta|$ is small ($|\delta| < 0.1$ Å) or large ($|\delta| > 0.5$ Å) where the displacement coordinate $\delta = R_{O^*H}\text{-}R_{O^\wedge H}$. Here R_{O^*H} and $R_{O^\wedge H}$ are the respective distances of the shared proton from O* and O^ the oxygen of the water molecule to which O* is hydrogen bonded to before PT occurs to O^. Several transitions of the intervening H atom occurred back and forth between these two oxygen atoms were observed before PT is complete. A newly formed four coordinated hydroxide ion on O^ is produced by hydrogen bonding with a water molecule in the vicinity (seen in Fig. 4(c)(iii)) when PT ends. Alternatively, successive proton transfers proceed through three-coordinated intermediates accompanied by solvent reorganization that must occur before proton transfer (see Fig. 6(b)). During a chain of successive PTs, the three coor-

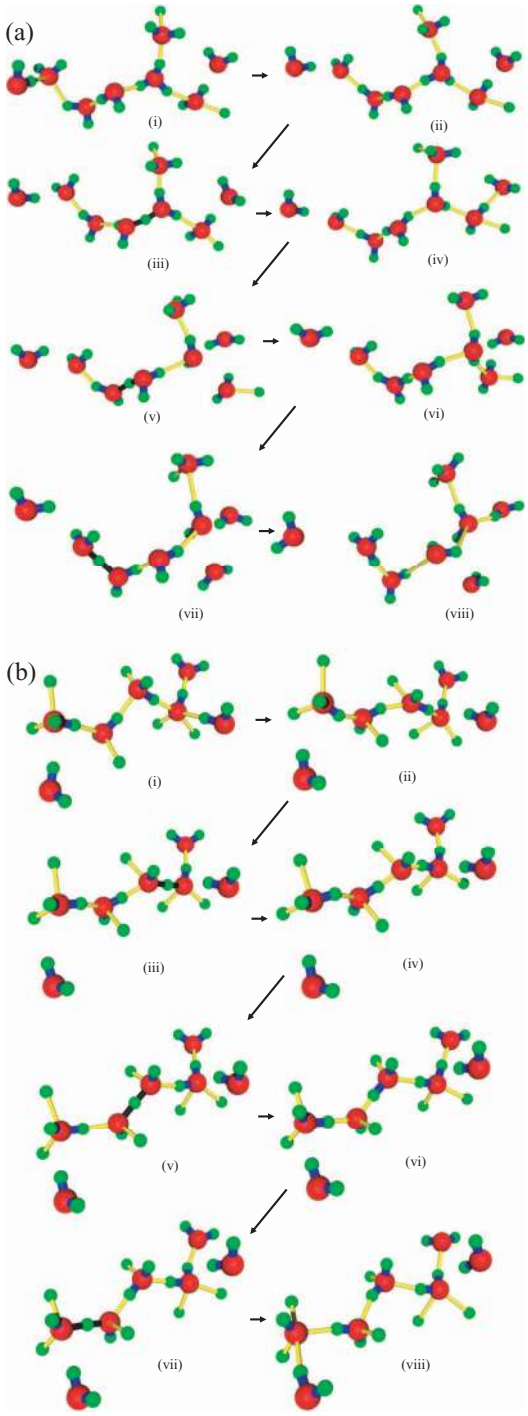

FIG. 6. (a) Representative configurations showing the mechanism of **successive** proton transfers leading to the transport of a hydrogen ion in a simulation of one H_3O^+ ion in 215 water molecules using the sOSS2 potential. (i) H_3O^+ ion stabilized as a three-coordinated Eigen complex $H_3O^+(H_2O)_3$ with a water molecule in the second solvation shell. (ii) Loss of water in the second solvation shell in (i). (iii) The formation of the Zundel intermediate $H_5O_2^+$. (iv) Completion of proton transfer *via* the Zundel intermediate to form a new H_3O^+ ion. Repetition of (iii)-(iv) in (v)-(vi) and (vii)-(viii). (b) Representative configurations of OH^- ion showing the mechanism of **successive** proton transfer leading to the transport of the hydroxide ion in a simulation of one OH^- ion in 215 water molecules using the sOSS2 potential. (i) $OH^-(H_2O)_{4.6}$ complex showing four coordination of OH^- and an additional H-bonded water molecule accepted 60% of the time by H of OH^- (ii) $OH^-(H_2O)_3$ intermediate showing three coordination of OH^- by loss of water. (iii) The formation of the Zundel-like transition state $H_3O_2^-$. (iv) Completion of proton transfer via $OH^-(H_2O)_3$ intermediate to form new OH^- ion. Repetition of (iii)-(iv) in (v)-(vi) and (vii)-(viii). The final structure of OH^- in (viii) is $OH^-(H_2O)_{4.6}$ complex.

dinated OH^- is dominant. PT ends when the final structure is the stable hyper-coordinated complex. For the hydroxide ion, successive PT begins and ends with the hyper-coordinated complex. The mechanism is in broad agreement with previous studies AIMD studies at room temperature using the BLYP functional.[3,33,39]

The evidence for hyper-coordination comes from left panel of Fig. 4(d) which shows that for large $|\delta| > 0.5$, the oxygen O* of the hydroxyl ion accepts on average four hydrogen bonds and donates one 60% of the time (coordination number $n_{O^*H} \sim 4.6$). Visual observations (configurations (i) and (iii) in Fig. 4(c)) show that the four hydrogen atoms are nearly in a plane slightly below the oxygen atom of the hydroxyl ion. When $|\delta| < 0.1$ (right panel of Fig. 4(d)) the OH^- ion is in a Zundel-like transition state, the first peak in the conditional pair correlation function g_{O^*O} present at 2.73 Å when $\delta > 0.5$ Å is split into two peaks, one at 2.43 Å which is equal to the O*-O distance the Zundel-like complex and the other at 2.81 Å due to the presence of an oxygen atom in the first solvation of O*. This splitting does not seem to have been observed in the AIMD study of Tuckerman *et al.* (see Fig. 2(b) of Ref. 3). The first intra-molecular peak in the O*-H pair correlation function g_{O^*H} at 0.99 Å for $\delta > 0.5$ Å also splits into two peaks at 0.98 Å and 1.21 Å, respectively; the second peak corresponding to the OH distance in the Zundel-like transition state. This splitting is observed in AIMD simulations of Tuckerman *et al*.[3]

The free energy profile F((δ) for proton transfer within the Zundel-like states for the basic solutions at 0.26 M was constructed from the normalized probability distributions P(δ)) and $F(\delta) = -kT \ln P(\delta)$ shown in Fig. 5(a) with the corresponding profile for the H^+ ion. The free energy barrier is 0.23 kcal/mol compared to 0.34 kcal/mol reported in Ref. 44; the barrier for the H^+ ion, as noted earlier, is lower and about 0.13 kcal/mol. The barrier height for PT transfer for the OH^- is quite still small indicating considerable proton delocalization.

In spite of the slightly larger barrier height and longer trajectory (~0.3 Å) for proton transfer across Zundel-like complex of the OH^- ion, the shuttling frequency is greater for the OH-ion than for the H^+ (compare middle and lower panels of Fig. 5(b)). Since the underlying mechanism of structural diffusion is proton transfer, fewer trajectories are successful in eventually leading to proton transfer in the basic solution (PT to the OH^- ion) than in the acidic solution (PT from the H_3O^+ ion). Comparison of the middle and upper panels of Fig. 5(b) shows that the frequency of successful PT events for the OH^- ion is less than the frequency of proton shuttling across the Zundel-like complex. This implies that the rate of structural diffusion in OH^- ion is determined by a factor besides the proton transfer rate across the Zundel-like complex. One such factor is the structural reorganization that must take place for PT to occur.

Large systems present no special difficulties in our simulations, and we observed several successive PT events in our study of the diffusion of H^+ and OH^- in 215 water molecules, in which each PT step, except the last, takes place after a time delay for solvent rearrangement and proton rattling.[33] Since the barriers are low, the dynamics of PT in aqueous solution

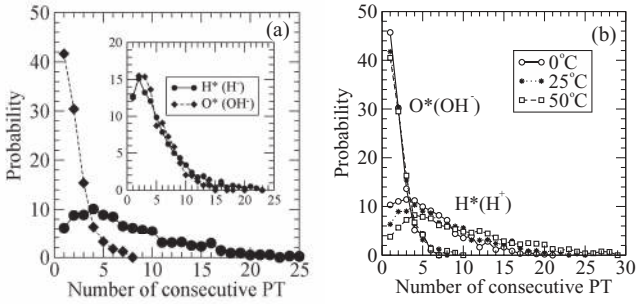

FIG. 7. (a) Probability distributions of consecutive PT jumps within 1 ps *vs*. their number at 298 K. The inset shows the distributions for consecutive jumps within the average time between jumps (0.72 ps for H^+ and 2.52 ps for OH^- ions, respectively, see text). (b) Probability distributions of consecutive PT jumps within 1 ps *vs*. their number as a function of temperature.

is governed by this time delay; the average time between two PT events at room temperature is 0.72 ps in the solution containing a single H^+ ion, and 2.52 ps in the solution with a single OH^- ion. Over the same time interval more successive PT events occur in the solution containing an excess H^+ ion than in the solution with an extra OH^- ion. The probabilities of a single isolated PT are 0.062 and 0.418, respectively, for the H^+ and OH^- ions at 298 K, demonstrating that successive PTs are a more likely to occur in the diffusion of the H^+ ion than in OH^- ion diffusion in aqueous solution. The dynamical asymmetry of PT transfer underlying the structural diffusion of H^+ and OH^- ions in water is clearly visible in the probability distributions of consecutive PT jumps each within 1 ps (Fig. 7(a)). When the 1 ps time delay is replaced by the average time between jumps (0.72 ps for the H^+ ion and 2.52 ps for the OH^- ion), the probability distribution functions are nearly coincident (inset of Fig. 7(a)). This suggests that the PT step is similar for both ions, but that it is modulated by different structural rearrangements of the solvated ions and the solvent between successive PT steps.

The structural rearrangements and associated time delays are different for H^+ and OH^- ions, and are reflected in the large difference in their mobilities. Successive proton transfers shown in Fig. 6(a) suggest a concerted mechanism for H^+ ion transport involving a reduction in the coordination number of a water molecule in the solvation shell of H_3O^+ before proton transfer occurs (panels (iv) and (v) in Fig. 6(a)).[1,34,70,71]

The average time between successive PT events changes with the temperature; it is larger (0.89 ps at 0 °C) at lower and smaller (0.62 ps at 50 °C) at higher temperatures than at 25 °C (0.72 ps) for a H^+ ion in 215 water molecules. The corresponding delay times for a OH^- ion in solution are 3.04 ps at 0 °C and 2.23 ps at 50 °C, respectively, in contrast to 2.52 ps at 25 °C, following the same trends as the H^+ ion. Since the probabilities of consecutive PTs increase with the temperature, the probabilities of a single PT are smaller at higher temperatures and larger at lower temperatures (Fig. 7(b)). When the 1 ps time delay is replaced by the average time between jumps, the jump probability distributions are nearly the same and similar to the inset of Fig. 7(a) at 298 K.

IV. REORIENTATION DYNAMICS OF THE OH^- ION

The relaxation times for the reorientation of an OH^- ion are difficult to determine because of PT events that occur on almost the same time scale, which is about 2.5 ps at room temperature. However, there is a distribution of times scales for PT, and we can compute the orientation correlation function $\langle P_2[\mathbf{u}(t)\cdot\mathbf{u}(0)]\rangle$ for the unit vector $\mathbf{u}(t)$ along the OH bond of the hydroxide ion from trajectories for which no PT events occur over times long enough to enable the relaxation time to be calculated. The relaxation times for reorientation are plotted as a function of the inverse temperature in Fig. 2 and coincide with the relaxation times for the OH bond of water at high temperatures, but deviate sharply from them below 290 K, in agreement with charge-transfer-to-solvent (CTTS) experiments[28] and a MD simulation study[72] of the OH^- ion in a non-dissociating model for water. There are then two activation energies (Table II), suggesting at least two different structures for the solvated hydroxide ion dominant at higher and lower temperatures respectively. This agrees with CTTS experiments that probe OH^- ions in water,[28] and is interpreted as arising from an increase in probability of $OH^-(H_2O)_3$ structure and a corresponding decrease in the probabilities of hyper-coordinated structures $OH^-(H_2O)_{4.6}$ with rise in temperature. This shift would also affect the rate of proton transfer and the mobility of the hydroxide ion.

V. THE MOBILITY OF H^+ AND OH^- IONS IN WATER

To monitor the sequence of PT events in the calculation of the diffusion coefficients, the index numbers of the transferred proton H* in the solution with the excess proton, and the oxygen O* of the hydroxide ion to which the proton was transferred in the solution with an excess hydroxide ion were recorded every 0.01 ps during each 100 ps block of time steps in our MD simulations (see Fig. 8). In the solution with the excess OH^- ion, O* moves in a direction opposite to that of proton transfer. In Fig. 5(b) we have shown the jump distances of O* and H* plotted against the time step. The smaller jump distances of H* (~0.25 Å) or O* (~0.06 Å) correspond to no change in index number and includes rattling while the larger jump distances of ~1.78 Å for H* and ~2.68 Å for O* imply a change in the index number indicating net structural diffusion.

The diffusion coefficients of the hydrogen and hydroxide ions were calculated from MSD for H* and O*, respectively,

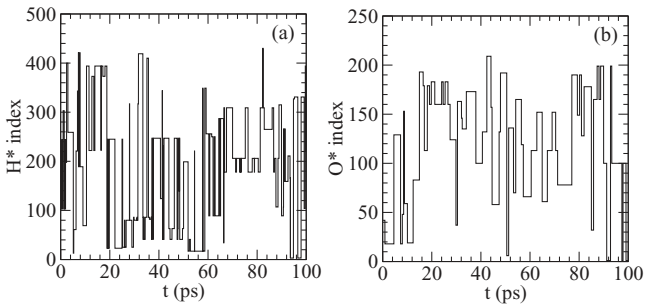

FIG. 8. Change in index numbers of (a) H* of H^+ ion and (b) O* of OH^- ion as a function of time.

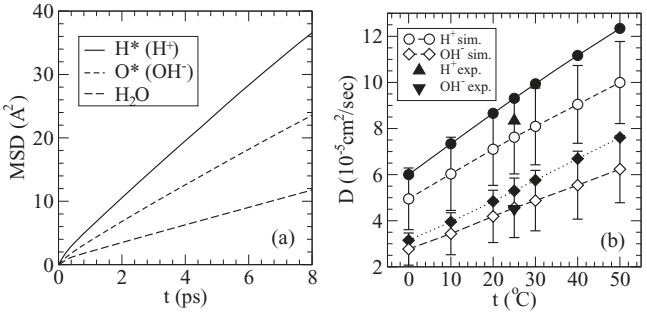

FIG. 9. (a) Mean square displacement of H* of H^+ ion, O* of OH^- ion and water at 298.15 K. (b) Diffusion coefficient of the H^+ and OH^- ion as a function of temperature (i) calculated from the sOSS2 model (○ for H^+ and ◇ for OH^-) at 0.26 M, (ii) experimental results (Ref. 77) at infinite dilution (● for H^+ and ◆ for OH^-) and (iii) experimental results (Refs. 74 and 76) for 0.26 M HCl and NaOH solutions at 298.15 K (▲ for H^+ and ▼ for OH^-).

for proton transfer events in 215 water molecules. We average over 60 and 100 blocks, respectively, for H* and O* and plot the MSD as a function of time in Fig. 9(a). The plots are linear and it is obvious that the slope for the hydroxide ion is smaller than that for the hydrogen ion in agreement with experiment. The diffusion coefficients calculated from the slopes are 7.62 × 10^{-5} cm^2/s for the hydrogen ion and 4.56 × 10^{-5} cm^2/s for the hydroxide ion at 298.15 K. The concentration of a single H^+ or OH^- ion in 215 water molecules is 0.26 M. The experimental diffusion coefficients of the H^+ and OH^- at infinite dilution are 9.31 × 10^{-5} cm^2/s and 5.30 × 10^{-5} cm^2/s, respectively, at 298 K.[59]

We can also estimate the diffusion coefficients D from the average PT jump distances (d) shown in Fig. 8 and the average time (τ) between successive jumps using $D \sim \langle d^2\rangle/6\tau$.[73] For H* we find $D \sim (1.78\ Å)^2/6\ (0.72\ ps) = 7.33 \times 10^{-5}$ cm^2/s and for O* we obtain $D \sim (2.68\ Å)^2/6\ (2.52\ ps) = 4.75 \times 10^{-5}$ cm^2/s. These numbers are close to our calculations of the diffusion coefficients from the MSD in Fig. 9(a).

The agreement between our simulations and the experimental results at infinite dilution is already very good but the comparison should be with the diffusion coefficients of H^+ and OH^- ion in 0.26 M HCl and NaOH, respectively, since the sodium and chloride ions at this concentration were the counter-ions in our simulations. The ion diffusion coefficients were calculated from the experimentally determined equivalent conductances Λ of HCl and NaOH at 0.26 M (37.8 mS m^2/mol and 21.2 mS m^2/mol (Refs. 74 and 75), respectively) using $D_i = \Lambda_i RT/z_i^2F^2$ ($\Lambda_i = t_i\Lambda$: equivalent ion conductance, z_i: valence, F: Faraday constant) after multiplying Λ for each electrolyte by the corresponding transport numbers ($t_{H^+} = 0.82$ and $t_{OH^-} = 0.8$ at 298 K) which are nearly constant.[75,76] The experimental diffusion coefficients are 8.24 × 10^{-5} cm^2/s for H^+ ion and 4.51 × 10^{-5} cm^2/s for the OH^- ion at 0.26 M in excellent agreement with our simulations (7.62 × 10^{-5} cm^2/s for the H^+ ion and 4.56 × 10^{-5} cm^2/s for the OH^- ion) using the sOSS2 model (see Fig. 9(b)). We note however that nuclear quantum effects are not explicitly included in our study.

Repeating the calculations at temperatures from 0 to 50 °C, the diffusion coefficients of both ions were found to

increase almost linearly with temperature in agreement with the trends shown by experimental results extrapolated to infinite dilution[77] (see Fig. 9(b)). The difference in mobilities of H^+ and OH^- ions persists and our calculations are in good agreement with experiment, assuming that the corrections for the concentration (0.26 M) remain small. This suggests that the sOSS2 potential is an excellent model for the hydrated H^+ and OH^- ions as well as for bulk water in this temperature range.

The activation energies for the diffusion of H^+ and OH^- ions, calculated from the Arrhenius equation $D = D_0 \exp(-E_{trans}/RT)$, are 10.3 kJ/mol and 12 kJ/mol, respectively, in excellent agreement with the experimental values of 10.6 kJ/mol and 12 kJ/mol, respectively, calculated from the experimental data at infinite dilution between 0 and 50 °C (Refs. 60 and 61), see Table I.

VI. CONCLUSIONS

Classical MD simulations using a scaled dissociating model potential (sOSS2) for liquid water provide unambiguous and clear pictures of the hydrated OH^- and H^+ ions and a computationally fast, accurate, and robust method of studying PT reactions in aqueous solutions. The simulations do not require large amounts of computational time or resources and can therefore be easily extended to large systems.

The model supports the EZE mechanism of proton transfer in acidic solutions and the transient hyper-coordination of the hydroxide ion in weakly basic solutions at room temperature.[1–6,34,35,38–44] The proportions of three-, four-, and hyper-coordinated solvation of the hydroxide ion change with temperature. Large numbers of successive PT events were observed, which enabled us to determine accurately the relative and absolute mobilities of hydrogen and hydroxide ions in aqueous solution, and their temperature dependence between 0 and 50 °C. Differences between the mobilities of these ions are traced to differences in the solvation structures and to different time delays for solvent reorganization of hydrated H^+ and OH^- ions before PT occurs, thereby breaking the hole-particle symmetry of the dynamics of proton transfer in H^+ and OH^- ions.[50,51] Nuclear quantum effects[2,3,44] are neglected in our study and future work could involve optimization of scaling to include these effects.

The sOSS2 model potential for liquid water and computational methods for PT discussed here could be adapted to study acid-base chemistry and large scale simulations of proton transfer reactions in solution, at interfaces[40,78] and in water filled nanopores.[40,79–81] The method of scaling the OSS2 potential could also be refined and applied to other interatomic potentials derived from *ab initio* quantum mechanical studies of a few molecules for use in large scale simulation studies of the bulk phase.

ACKNOWLEDGMENTS

S.H.L. was supported by the National Research Foundation of Korea Grant funded by the Korean Government (MEST) (NRF-2010-0023062) and J.C.R. was supported by a National Science Foundation (NSF) Grant No. CHE 0549187.

[1] M. E. Tuckerman, K. Laasonen, M. Sprik, and M. Parrinello, J. Chem. Phys. **103**, 150 (1995).
[2] D. Marx, M. E. Tuckerman, J. Hutter, and M. Parrinello, Nature (London) **397**, 601 (1999).
[3] M. E. Tuckerman, D. Marx, and M. Parrinello, Nature (London) **417**, 925 (2002).
[4] B. Chen, J. M. Park, I. Ivanov, G. Tabacchi, M. L. Klein, and M. Parrinello, J. Am. Chem. Soc. **124**, 8534 (2002)
[5] D. Asthagiri, L. R. Pratt, J. D. Kress, and M. A. Gomez, Proc. Natl. Acad. Sci. U.S.A. **101**, 7229 (2004).
[6] D. Bucher, A. Gray-Weale, and S. Kuyucak, J. Chem. Theory Comput. **6**, 2888 (2010).
[7] A. Warshel and R. M. Weiss, J. Am. Chem. Soc. **102**, 6218 (1980).
[8] R. Vuilleumier and D. Borgis, J. Chem. Phys. **111**, 4251 (1999).
[9] J. Lobaugh and G. A. Voth, J. Chem. Phys. **104**, 2056 (1996).
[10] U. W. Schmidt and G. A. Voth, J. Phys. Chem. B. **102**, 5547 (1998).
[11] T. J. F. Day, A. V. Soudakov, M. Cuma, U. W. Schmidt, and G. A. Voth, J. Chem. Phys. **117**, 5839 (2002).
[12] I. S. Ufimstev, A. G. Kalinichev, T. J. Martinez, and R. J. Kirkpatrick, Phys. Chem. Chem. Phys. **11**, 9420 (2009).
[13] M. E. Selvan, D. J. Keffer, S. Cui, and S. J. Paddison, J. Phys. Chem. C **14**, 11965 (2010).
[14] F. Bruni, M. A. Ricci, and A. K. Soper, J. Chem. Phys. **114**, 8056 (2001).
[15] A. Botti, F. Bruni, S. Imberti, M. A. Ricci, and A. K. Soper, J. Chem. Phys. **119**, 5001 (2003).
[16] A. Botti, F. Bruni, S. Imberti, M. A. Ricci, and A. K. Soper, J. Chem. Phys. **120**, 10154 (2004).
[17] S. Imberti, A. Botti, F. Bruni, G. Cappa, M. A. Ricci, and A. K. Soper, J. Chem. Phys. **122**, 194509 (2005).
[18] A. Botti, F. Bruni, S. Imberti, M. A. Ricci, and A. K. Soper, J. Mol. Liq. **117**, 77 (2005).
[19] A. Botti, F. Bruni, S. Imberti, M. A. Ricci, and A. K. Soper, J. Mol. Liq. **117**, 81 (2005).
[20] S. E. McLain, S. Imberti, A. K. Soper, A. Botti, F. Bruni, and M. A. Ricci, Phys. Rev. B **74**, 0942201 (2006).
[21] T. Megyes, S. Balint, T. Grosz, T. Radnai, L. Bakó, and P. Sipsos, J. Chem. Phys. **128**, 044501 (2008).
[22] C. D. Cappa, J. D. Smith, B. M. Messer, R. C. Cohen, and J. Saykally, J. Phys. Chem. A **111**, 4776 (2007).
[23] K. S. Asmis, N. L. Privonka, G. Santambrogio, M. Brummer, C. Kaposta, D. M. Neumark, and L. Wöste, Science **299**, 1375 (2003).
[24] M. Rini, B. Z. Magnus, E. Pines, and E. T. J. Nibbering, Science **301**, 493 (2003).
[25] O. F. Mohamed, D. Pines, J. Dreyer, E. Pines, and E. T. J. Nibbering, Science **310**, 83 (2005).
[26] J. M. Headrick, E. G. Diken, R. S. Walters, N. I. Hammer, R. A. Christie, J. Cui, E. M. Myshakin, M. A. Duncan, M. A. Johnson, and K. D. Jordan, Science **308**, 1765 (2005).
[27] S. Woutersen and H. J. Bakker, Phys. Rev. Lett. **96**, 138305 (2006).
[28] J. Thøgersen, S. K. Jensen, C. Petersen, and S. Keiding, Chem. Phys. Lett. **466**, 1 (2008).
[29] S. T. Roberts, P. B. Petersen, K. Ramasesha, A. Tokmakoff, I. S. Ufimtsev, and T. J. Martinez, Proc. Natl. Acad. Sci. U.S.A. **106**, 15154 (2009).
[30] S. G. Olesen, T. L. Guasco, J. R. Roscioli, and M. A. Johnson, Chem. Phys. Lett. **509**, 89 (2011).
[31] S. T. Roberts, K. Ramasesha, P. B. Petersen, A. Mandal, and A. Tokmakoff, J. Phys. Chem. A **115**, 3957 (2011).
[32] E. F. Aziz, N. Ottosson, M Faubel, I. V. Hertel, and B. Winter, Nature (London) **455**, 89 (2008).
[33] A. Chandra, M. E. Tuckerman, and D. Marx, Phys. Rev. Lett. **99**, 145901 (2007).
[34] N. Agmon, Chem. Phys. Lett. **244**, 456 (1995).
[35] N. Agmon, Isr. J. Chem. **39**, 493 (1999).
[36] J. Hynes, Nature (London) **397**, 565 (1999).
[37] N. Agmon, Chem. Phys. Lett. **319**, 247 (2000).
[38] R. Ludwig, Angew. Chem., Int. Ed. **42**, 258 (2003).
[39] M. E. Tuckerman, A. Chandra, and D. Marx, Acc. Chem. Res. **39**, 151 (2006).
[40] G. A. Voth, Acc. Chem. Res. **39**, 143 (2006).

[41]J. M. J. Swanson, C. M. Maupin, H. Chen, M. K. Petersen, J. Xu, Y. Wu, and G. A. Voth, J. Phys. Chem. B **111**, 4300 (2007).
[42]H. Lapid, N. Agmon, M. K. Petersen, and G. A. Voth, J. Chem. Phys. **122**, 014506 (2005).
[43]O. Markovitch, H. Chen, S. Izvekov, F. Paesani, G. A. Voth, and N. Agmon, J. Phys. Chem. B **112**, 9456 (2008).
[44]D. Marx, A. Chandra, and M. E. Tuckerman, Chem. Rev. **110**, 2174 (2010).
[45]D. Asthagiri, L. R. Pratt, J. D. Kress, and M. A. Gomez, Chem. Phys. Lett. **380**, 530 (2003).
[46]E. E. Dahlke and D. G. Truhlar, J. Phys. Chem. B **109**, 15677 (2005).
[47]J. VandeVondele, F. Mohamed, M. Krack, J. Hutter, M. Sprik, and M. Parinello, J. Chem. Phys. **122**, 014515 (2005).
[48]I. S. Ufimstev, A. G. Kalinchev, T. J. Martinez, and R. J. Kirkpatrick, Chem. Phys. Lett. **442**, 128 (2007)
[49]L. Ojamäe, I. Shavitt, and S. J. Singer, J. Chem. Phys. **109**, 5547 (1998).
[50]H. L. Lemberg and F. H. Stillinger, J. Chem. Phys. **62**, 1677 (1975).
[51]F. H. Stillinger and C. W. David, J. Chem. Phys. **73**, 3384 (1980).
[52]T. A. Weber and F. H. Stillinger, J. Chem. Phys. **77**, 4150 (1982).
[53]S. H. Lee and J. C. Rasaiah, Mol. Simul. **36**, 69 (2010).
[54]G. Stell, "Fluids with long-range forces," in *Statistical Mechanics Part A*, Equilibrium Techniques, Modern Theoretical Chemistry Vol. 5, edited by B. J. Berne (Plenum, New York, 1977), Chap. 2.
[55]G. Stell, J. C. Rasaiah, and H. Narang, Mol. Phys. **27**, 1393 (1974).
[56]W. G. Hoover, Phys. Rev. A **31**, 1695 (1985).
[57]W. C. Swope, H. C. Andersen, P. H. Berens, and K. R. Wilson, J. Chem. Phys. **76**, 637 (1982).
[58]S. H. Lee, Bull. Korean Chem. Soc. **22**, 847 (2001).
[59]P. Atkins and J. D. Paula, *Physical Chemistry*, 7th ed. (Freeman, New York, 2002), p. 1104.
[60]M. Holz, S. R. Heil, and A. Sacco, Phys. Chem. Chem. Phys. **2**, 4740 (2002).
[61]A. J. Easteal, W. E. Price, and L. A. Woolf, J. Chem. Soc., Faraday Tans. 1 **85**, 1091 (1985).
[62]D. A. Turton and K. Wynne, J. Chem. Phys. **128**, 154516 (2008).
[63]A. Luzar and D. Chandler, Nature (London) **379**, 55 (1996).
[64]D. Laage and J. T. Hynes, Science **311**, 832 (2006).
[65]D. Laage and J. T. Hynes, Proc. Natl. Acad. Sci. U.S.A. **104**, 11167 (2007).
[66]D. Laage and J. T. Hynes, J. Phys. Chem. B **112**, 14230 (2008).
[67]A. K. Soper, Chem. Phys. **258**, 121 (2000).
[68]H. J. C. Berendsen, J. R. Grigera, and T. P. Straatsma, J. Phys. Chem. **91**, 6269 (1987).
[69]S. Koneshan, J. C. Rasaiah, and L. X. Dang, J. Chem. Phys. **114**, 7544 (2001).
[70]M. E. Tuckerman, K. Laasonen, M. Sprik, and M. Parrinello, J. Phys. Chem. **99**, 5749 (1995).
[71]T. C. Berkelbach, H.-S. Lee, and M. E. Tuckerman, Phys. Rev. Lett. **103**, 238302 (2009).
[72]X. Sun, S. Yoo, S. S. Xantheas, and L. X. Dang, Chem. Phys. Lett. **481**, 9 (2009).
[73]Z. Luz and S. Meiboom, J. Am. Chem. Soc. **86**, 4768 (1964)
[74]R. H. Stokes, J. Phys. Chem. **65**, 1242 (1961).
[75]C. H. Hamann, A. Hamnett, and W. Vielstich, *Electrochemistry*, 2nd ed. (Wiley VCH, Berlin, 2007).
[76]H. S. Harned and B. B. Owen, *The Physical Chemistry of Electrolyte Solutions*, 3rd ed. (Reinhold, New York, 1958).
[77]T. S. Light, S. Licht, A. C. Bevilacqua, and K. R. Morash, Electrochem. Solid-State Lett. **8**, E16 (2008).
[78]C. J. Mundy, I.-F. W. Kuo, M. E. Tuckerman, H.-S. Lee, and D. J. Tobias, Chem. Phys. Lett. **481**, 2 (2009).
[79]J. C. Rasaiah, S. Garde, and G. Hummer, Ann. Rev. Phys. Chem. **59**, 713 (2008).
[80]G. Hummer, J. C. Rasaiah, and J. P. Noworyta, Nature (London) **414**, 188 (2001).
[81]C. Dellago, M. M. Naor, and G. Hummer, Phys. Rev. Lett. **90**, 105902 (2003).